On the Accuracy of a Video-Based Drill-Guidance Solution for Orthopedic and Trauma Surgery: Preliminary Results

Jessica Magaraggia[1,2], Gerhard Kleinszig[2], Wei Wei[2], Markus Weiten[2], Rainer Graumann[2], Elli Angelopoulou[1,3], Joachim Hornegger[1,3]

[1]Pattern Recognition Lab, University of Erlangen-Nuremberg, Erlangen, Germany
[2]Siemens AG, Healthcare Sector, Erlangen, Germany
[3]Erlangen Graduate School in Advanced Optical Technologies (SAOT)

ABSTRACT

Over the last years, several methods have been proposed to guide the physician during reduction and fixation of bone fractures. Available solutions often use bulky instrumentation inside the operating room (OR). The latter ones usually consist of a stereo camera, placed outside the operative field, and optical markers directly attached to both the patient and the surgical instrumentation, held by the surgeon. Recently proposed techniques try to reduce the required additional instrumentation as well as the radiation exposure to both patient and physician. In this paper, we present the adaptation and the first implementation of our recently proposed video camera-based solution for screw fixation guidance. Based on the simulations conducted in our previous work, we mounted a small camera on a drill in order to recover its tip position and axis orientation w.r.t our custom-made drill sleeve with attached markers. Since drill-position accuracy is critical, we thoroughly evaluated the accuracy of our implementation. We used an optical tracking system for ground truth data collection. For this purpose, we built a custom plate reference system and attached reflective markers to both the instrument and the plate. Free drilling was then performed 19 times. The position of the drill axis was continuously recovered using both our video camera solution and the tracking system for comparison. The recorded data covered targeting, perforation of the surface bone by the drill bit and bone drilling. The orientation of the instrument axis and the position of the instrument tip were recovered with an accuracy of $1.60 \pm 1.22°$ and 2.03 ± 1.36 mm respectively.

Keywords: Video-guided method, Real-time guidance, Orthopedic and Trauma Surgery, Drill Sleeve

1. INTRODUCTION

Fracture reduction and fixation are still nowadays usually performed on a free-hand basis. Intra-operatively, the physician monitors the result of the correct placement of implants and screws by means of X-ray images acquired by a C-arm. However, such X-ray imaging requires accurate C-arm alignment and repeated acquisitions at different angles. Complex configurations of screws and implants can be technically demanding w.r.t not only the surgical skills of the physician, but also the required X-ray acquisitions. This results in both an increased radiation exposure of the medical staff and a cumbersome procedure for correct alignment. Still, no comprehensive spatial information can be gained from solely 2-D imaging. Moreover, intra-operative monitoring by means of a C-arm allows for the detection of erroneous positioning just after the drilling has been already completed. This leads to an undesirable trial and error process. In fact, precise implant placement and accurate screw positioning plays a critical role in the success of the surgical procedure and the recovery of good locomotor function[1,2].

Several solutions have been developed in order to provide intra-operative guidance information to the physician. Optical navigation systems, like the VectorVision® from BRAINLAB AG. and Navigation System II from Stryker Inc., employ an infrared stereo camera placed outside the operative field and a set of markers attached to the instrument to be tracked. The main drawbacks are the required clear line-of-sight between the stereo camera and the markers and the bulky instrumentation that is introduced inside the OR, which constrains the free movement of the medical staff and in particular of the physician. Diotte et al.[3] exploited an augmented C-arm

The presented method is investigational use and is limited by U.S. law to investigational use. It is not commercially available in the U.S. and its future availability cannot be ensured.

Medical Imaging 2014: Image-Guided Procedures, Robotic Interventions, and Modeling, edited by David R. Holmes, Ziv R. Yaniv, Proc. of SPIE Vol. 9036, 903610 (2014) doi:10.1117/12.2043508; http://dx.doi.org/10.1117/12.2043508

and a modified Schanz screw to determine and visualize the tip position of the drilling guide by only exploiting camera images. However, such a solution requires the use of an augmented C-arm inside the OR. We recently proposed the use of a small video camera, which is directly placed on the surgical drill, and a set of markers that are rigidly fixed on a drill sleeve[4]. In such a setup the position of the camera and consequently of the instrument tip and axis, could be determined w.r.t the local coordinate system of the locking screw hole, where the drill sleeve is placed. However, only a feasibility analysis based on simulations was provided.

In this paper, we extend our previous work. We developed a new variant, built a first prototype and quantitatively evaluated its performance. We used a custom-made variable angle drill sleeve. Unlike the original work[4], we place our markers on the drill sleeve's handle (instead of the drill sleeve itself), thus ensuring a 3-D marker configuration during the entire drilling phase and not just during the targeting step. Based on our prior simulation results[4], this modification should result in a more accurate and robust position-feedback. Placement of the markers on the drill sleeve handle would further reduce the risk of contact with the surrounding tissues at the surgical site. Moreover, we exploited a real-time tracking system to provide a full analysis of the accuracy of our implemented setup. Our prototype: 1) provides 3-D position of the drill tip and axis w.r.t the reference coordinate system represented by the drill sleeve; 2) provides real-time position feedback with no radiation exposure; 3) would require minimal additional instrumentation inside the OR; 4) does not necessitate the use of an augmented C-arm; and 4) would not constrain the movement of the medical staff around the operating table.

2. METHODS

In this section, we describe our prototype and the evaluation setup we used for the quantitative performance analysis. We mounted a video camera on a drill as shown in Fig. 3(a). Once fixed, the relative position between the camera and the drill does not change.

2.1 Markers Positioning

The key problem, then, is to relate the position of the camera, and therefore of the instrument, to a meaningful reference system. We had previously suggested to use a drill sleeve for this purpose. Drill sleeves are already employed in the clinical workflow for several parts of the body, e.g. tibia, distal radius or feet. A physician uses a drill sleeve to prevent tissue wrapping around the drill bit and to avoid contact between the drill bit and ligaments and tendons that surround the surgical site. Furthermore, drill sleeves constrain the direction of the drilling, allowing for a more controlled procedure. Therefore, a camera-based solution that exploits drill sleeves is designed to be integrated into a standard fracture reduction procedure without alteration of the surgical workflow. Thanks to the dedicated implant-drill sleeve interfaces, the position of the drill sleeve w.r.t the implant can be determined when it is rigidly placed at one of the locking holes of the implant. Moreover, the drill bit position w.r.t the patient could also be recovered. For this purpose, the implant should be registered to intra-operatively acquired X-ray images, via a 2D-3D registration algorithm e.g.[5,6].

In[4] it was suggested to place the markers on a planar ring attached to the drill sleeve's upper aperture. Such a marker placement can be used to relate the position of the camera, and consequently of the drill bit, to the implant. However, it has some drawbacks that limit its applicability: a 3-D marker configuration is not available during the drilling procedure; the working space for the placement of the markers is very small, negatively affecting the accuracy of marker detection; the ring increases the volume of the drill sleeve in its lowest part, thus increasing the risk of unwanted contact with the surrounding body structures.

To overcome these limitations, we now position the markers in a 3-D configuration on the handle of the drill sleeve instead of the drill sleeve itself, see Fig. 3(b). In our prototype, we used a custom-made variable-angle drill sleeve and a relative plate. Similar to the drill sleeves used in clinical practice, our drill sleeve allows the orientation of the drill bit up to $\pm 15^\circ$ w.r.t the plate normal at the locking hole. Free position of the drill bit within this range is allowed. We also used a custom-made marker holder, which can be rigidly fixed to the handle of the drill sleeve. Three square markers with binary coding[4,7] are attached to the holder in a 3-D configuration. Each square marker has a dimension of 8×8 mm. Some examples of images acquired with our camera are shown in Fig. 1. Clearly, depending on the position of the drill, markers can lie outside the Field of View (FOV) of

Jessica Magaraggia: jessica.magaraggia@cs.fau.de

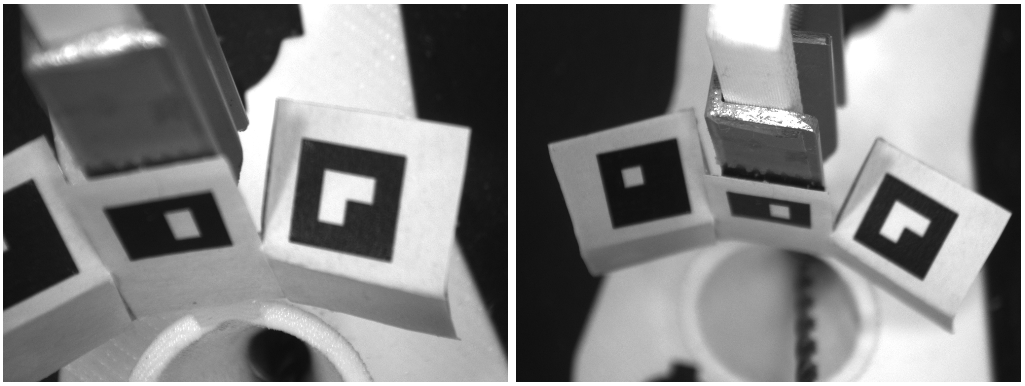

(a) (b)

Figure 1. Sample images recorded by our camera.

the camera or be affected by strong perspective distortion, impairing correct marker detection. If one marker is outside the FOV, our designed marker arrangement, still ensures a 3-D feature-arrangement. Nevertheless, thorough evaluation is required in order to have an understanding of the accuracy that such a setup could deliver.

2.2 Camera Pose Recovery

Algorithms for camera pose recovery can be exploited in order to recover the camera position and as a consequence also the drill bit position. As mentioned in the previous sections, the proposed marker layout ensures a 3-D configuration of the features that are used for the recovery of the camera pose. As previously proposed[4], markers are detected using an edge based algorithm and the PnP algorithm by Lu et al.[8] is used for camera pose recovery. In comparison, we decided to perform marker segmentation independently at each frame. No tracking was therefore included in the detection pipeline. The usage of solely frame-per-frame segmentation allows us to investigate the impact of a vibrating drill on the on-line segmentation and on the accuracy of the pose recovery. We expect the result of the marker detection to be affected by the motion blur introduced from the instrument vibrations. Critical is the situation, where no markers are detected. This can happen when all the markers fall outside the FOV of the camera, in case e.g. of a sudden and undesired hand movement or because the marker detection fails due to high image blur.

2.3 Setup of the Optical Tracking System

In order to investigate the accuracy that our prototype can deliver, we need to compare it with a meaningful ground truth. Our ground truth is provided by the Polaris Spectra (NDI, Ontario, Canada). The system is composed of a stereo camera and a set of passive markers, whose position can be tracked with a frequency rate up to 60Hz. More specifically, we rigidly attached our custom-made plate with the drill sleeve to a second plate, which is equipped with passive markers (see Fig. 3(b)). In the remainder of this paper, $\mathbf{S_M}$ and $\mathbf{S_P}$ will denote the coordinate system of the drill sleeve and of the passive markers on the plate respectively. Once fixed, the transformation $\mathbf{T_P^M}$ from $\mathbf{S_M}$ to $\mathbf{S_P}$ is known. At the location where our custom-made drill sleeve is positioned, a hole is present in the second plate. This allows free movement of the drill bit through the plate. We use the convention $\mathbf{T_j^i}$ to indicate the transformation that maps i to j.

A second set of passive markers is attached to the drill (see Fig. 3(a)). Its coordinate system is denoted as $\mathbf{S_A}$. Instrument calibration is performed in order to relate the position of the instrument tip and axis to $\mathbf{S_A}$. Calibration w.r.t $\mathbf{S_A}$ is performed in a manner similar to[9]. The instrument is then identified by an axis $\mathbf{v_A}$ and a point $\mathbf{P_T}$, the instrument tip, expressed in $\mathbf{S_A}$ as: $\{\mathbf{P_T}, \mathbf{v_A}\}_{\mathrm{S_A}}$.

2.4 Instrument Calibration

The calibration of our prototype w.r.t the camera coordinate system $\mathbf{S_C}$ is performed using a variant of the work presented in[10] that exploits quaternions. After calibration, the drill tip position and axis orientation are known w.r.t $\mathbf{S_C}$: $\{\mathbf{P_T}, \mathbf{v_A}\}_{\mathrm{S_C}}$. In [10] a calibration holder plate is used for the instrument calibration. In the

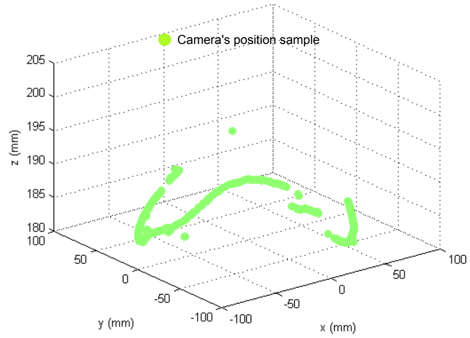

(a)

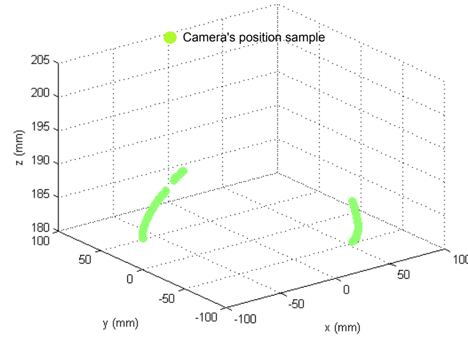

(b)

Figure 2. Instrument tip and axis calibration w.r.t $\mathbf{S_C}$. In a), all the collected camera positions are shown. In b), just the samples selected when running RANSAC outlier rejection are shown.

plate, an insertion guide is present in order to host the axis of the instrument in the direction orthogonal to the surface plate and the instrument tip at a predefined known position w.r.t the reference plate coordinate system $\mathbf{S_R}$. When the instrument is in place, it is manually rotated about its axis and the transformation matrix $\mathbf{T_C^R}$ from $\mathbf{S_R}$ to $\mathbf{S_C}$ is continuously calculated. From $\mathbf{T_C^R}$, also the instrument axis and tip position w.r.t $\mathbf{S_C}$ can be derived. In the end, a weighted average is used in order to obtain a final estimate of $\{\mathbf{P_T}, \mathbf{v_A}\}_{\mathrm{S_C}}$. However, the accuracy of the calibration was affected by the deviation of the instrument from its expected position due to the unbalanced weight of the instrument and the movement caused by the user.

To overcome this problem, we decided to use the prior information about the instrument movement. The instrument is expected to be rotated about its axis. This means that ideally, the trajectory described by the the origin of the camera coordinate system $\mathbf{S_C}$ has to lie on a circle. We can then first of all use RANSAC to estimate the optimal circle that fits the collected camera's position samples and get rid of the outliers. In Fig. 2(a) an example of the collected samples is shown. It is clear that deviations from the expected trajectory do occur. In Fig. 2(b), the result of the outlier rejection process is shown. Just the samples that do fit the estimated best trajectory are retained.

As suggested by Schmidt et al.[11], we can exploit a quaternion representation. At each camera position, the camera pose $\mathbf{T_R^C}$ is recovered. Afterward, given two position samples at the randomly chosen time stamps $\mathrm{t_i}$ and $\mathrm{t_j}$ in the collected sequence, we can calculate the relative rotation matrix $\mathbf{R_{ij}} = \mathbf{R_j^T}\mathbf{R_i}$ and express it in quaternion form: $\mathbf{q_{ij}} = (\cos(\theta/2), \sin(\theta/2)\mathbf{v_{ij}})$. According to this notation, $\mathbf{v_{ij}}$ represents the vector about which the rotation is performed and θ represents the angle of rotation. Since our instrument is thought to rotate about a fixed axis direction, all the possible $\mathbf{v_{ij}}$ ideally describe the same vector. As suggested in[11], we applied a fixed threshold $\theta_t = 15°$ for the rotation angle. For each couple of samples k that survives this selection step we calculate $\mathbf{T_C^R}$ and estimate the orientation of the instrument axis in the camera coordinate system $\mathbf{S_C}$: $\mathbf{v}_{\mathrm{C}}^{\mathbf{k}}$. The final estimation of the instrument axis $\overline{\mathbf{v_C}}$ is again obtained averaging all the N estimated $\mathbf{v}_{\mathrm{C}}^{\mathbf{k}}$ values (see Eq. 1)[10].

$$\overline{\mathbf{v_C}} = \frac{\sum_{k=1}^{\mathrm{N}} \mathbf{v_C^k}}{||\sum_{k=1}^{\mathrm{N}} \mathbf{v_C^k}||} \tag{1}$$

2.5 Estimation of the Instrument Tip and Axis in a Common Reference Frame

When the drill bit is positioned inside the drill sleeve, the markers are visible in the camera FOV. The camera pose, i.e. the transformation $\mathbf{T_M^C}$ from $\mathbf{S_C}$ to $\mathbf{S_M}$ is recovered using the algorithm of Lu et al.[8]. For each camera frame, we can then use the calculated $\mathbf{T_M^C}$ to determine the instrument position in $\mathbf{S_M}$: $\{\mathbf{P_T}, \mathbf{v_A}\}_{\mathrm{S_M}}$ as recovered from our video-camera In an analogous manner, we exploit the Polaris system, denoted by $\mathbf{S_S}$, to recover the instrument position in $\mathbf{S_P}$: $\{\mathbf{P_T}, \mathbf{v_A}\}_{\mathrm{S_P}}$ as recovered by our ground-truth. To this purpose, the transformation $\mathbf{T_P^A}$ is recovered as reported in Eq. 2.

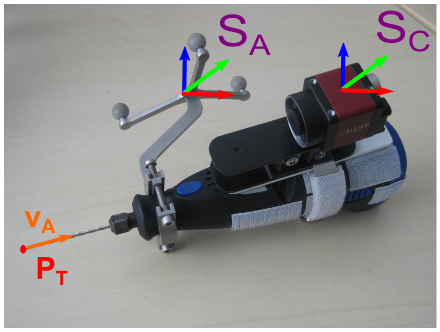

(a)

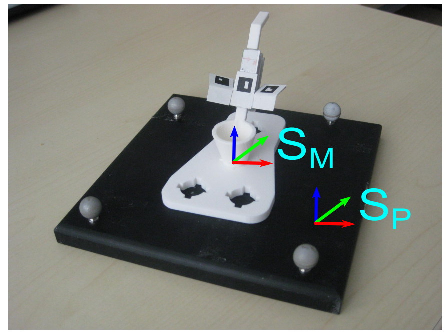

(b)

Figure 3. (a) Our drill with the attached camera and the reflective markers used for the ground-truth extraction. (b) Our custom-made drill sleeve on the reference plate.

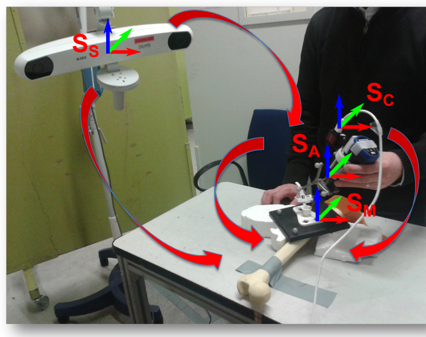

Figure 4. Our evaluation setup with relative coordinate systems is shown

$$\mathbf{T_P^A} = \mathbf{T_P^S}\mathbf{T_S^A} \tag{2}$$

$$\mathbf{T_P^C} = \mathbf{T_P^M}\mathbf{T_M^C} \tag{3}$$

The last step is to use the known $\mathbf{T_P^M}$ to express the instrument position recovered by the camera-based system in $\mathbf{S_P}$. The instrument position recovered once by our camera-based system and once by the Polaris tracker is now expressed in a common reference system, $\mathbf{S_P}$. Continuous comparison of the estimated instrument position is therefore possible.

For the image frames, for which no markers were detected, we assume no change in the instrument position. That is, if $\mathbf{I_i}$ and $\mathbf{I_{i-1}}$ are two images acquired at two successive time stamps $\mathrm{t_i}$ and $\mathrm{t_{i-1}}$, we assume $\{\mathbf{P_T}, \mathbf{v_A}\}_{\mathrm{S_{M,i}}} = \{\mathbf{P_T}, \mathbf{v_A}\}_{\mathrm{S_{M,i-1}}}$.

3. EXPERIMENTS AND RESULTS

For our experiments, we calibrated our camera-drill system as described in the previous section. In order to check the quality of our calibration, we performed a static measurement, while holding our instrument still by hand at a position where all the markers on the reference plate are visible. At the same time, the position of the instrument tip and of the drill axis where recorded using both our video-camera and the Polaris system for about 6 s. The accuracy of the tip position concerning our ground truth was 0.3 mm. The results of the calibration of our prototype are shown in Fig. 5, where we compare the tip position obtained with our video-camera system with the one delivered by the Polaris system (x and z direction are shown). The error obtained for the axis orientation is also shown. We got an error for the tip position of 0.54 ± 0.07 mm and an error for the axis orientation of $0.46 \pm 0.06°$. Referring to Fig. 5(a) and Fig. 5(b), we can already make some comments about the different response of the two system. Although our prototype delivers a tip position, that does constantly follow

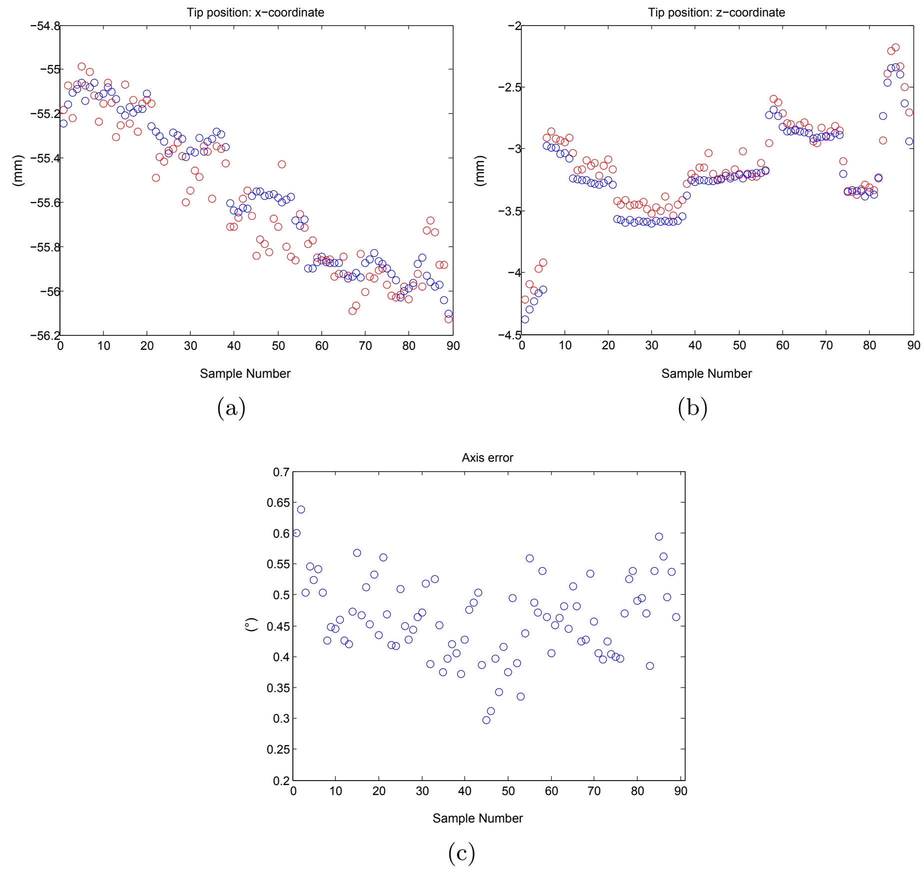

Figure 5. The comparison between the tip position obtained using our prototype and our ground truth in (a) the x and (b) z-axis is shown . In (c), the error obtained when comparing the axis orientation with the ground truth is also shown.

the position delivered by our ground truth, it appears less sensitive to small variations, smoothing out small and rapid variations produced by the natural hand shaking, while holding the instrument.

After calibration, we performed a dynamic test. We first fixed our reference plate on a dry bone as shown in Fig. 4. We then performed 19 drilling procedures, spanning the $\pm 15\,^\circ$ space allowed by the drill sleeve. Our average axis orientation was $11.07 \pm 3.05°$. The average depth of drilling was 22.68 ± 11.46 mm. No specific targets were defined, since we did not want to restrict our evaluation to a mere target-to-reach action. Our main goal is to perform an evaluation of the prototype accuracy in real-time. For each sequence, we: 1) positioned the drill inside our custom-made drill sleeve at a desired angle, 2) switched on the drill and both the video-camera and the Polaris tracker and 3) recorded the instrument position with both systems while drilling for a time-window of 10 s. The recorded time included therefore: 1) initial drill position, 2) hit and perforation of the surface of the bone and 3) deep advancement of the drill bit inside the dry bone. Our camera-based system delivered the instrument position at an average rate of 14 FPS at a image resolution of 768×1024 px. The tracking rate of the Polaris was set to 20 Hz.

For each frame, we calculated both the error in the instrument tip position and in the axis orientation according to:

$$e_\theta = arccos(\mathbf{v_{MP}} \cdot \mathbf{v_P}) \qquad\qquad e_{\mathrm{IT}} = \|\mathbf{P_{MP}} - \mathbf{P_P}\|_\mathbf{2} \tag{4}$$

where $\mathbf{v_{MP}}$ and $\mathbf{P_{MP}}$ are the estimated axis orientation and tip position obtained with our camera-based system expressed in $\mathbf{S_P}$, while $\mathbf{v_P}$ and $\mathbf{P_P}$ are the corresponding values obtained using the Polaris tracker, also expressed in $\mathbf{S_P}$. $\mathbf{v_{MP}}$ and $\mathbf{v_P}$ are unit vectors. The outcome of the 19 sequences is shown in Fig. 6.

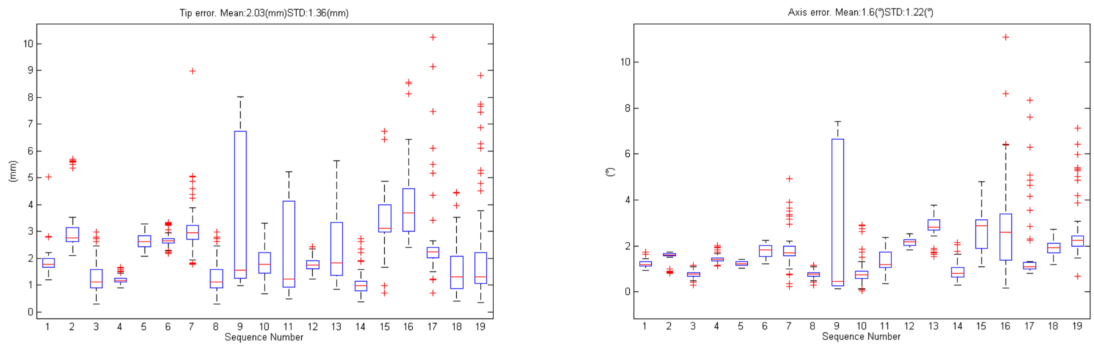

(a) (b)

Figure 6. In the figure, (a) tip position error (mm) and (b) axis orientation error (°) are shown for each drilling operation that was performed.

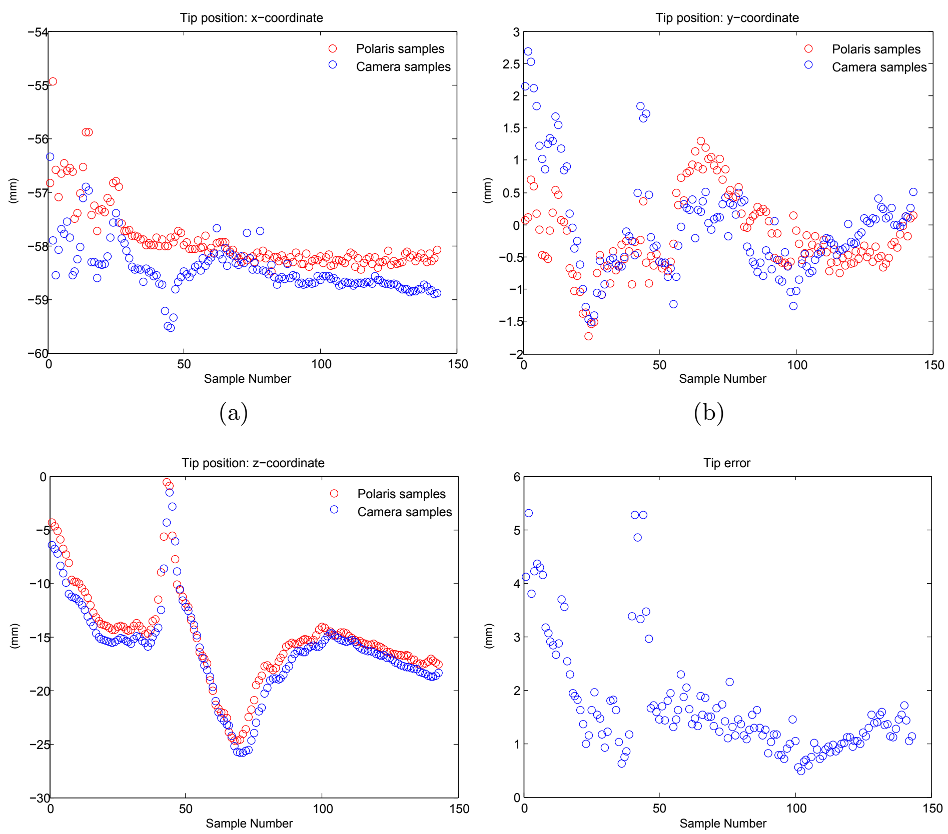

(c) (d)

Figure 7. In the figure, estimated tip positions along the (a) x, (b) y and (c) z-axis are shown. Samples obtained using our prototype are shown in blue, while our ground truth is depicted in red color. In (d) the tip error, calculated according to Eq. 4 is shown. The samples were obtained from a time-window of 10 s. and refer to the sequence nr. 18 in Fig. 6

An example of the accuracy of our method on one such recorded procedure is shown in Fig. 7. In particular, we show the comparison between our estimated tip position in the three direction axes x, y and z, and the corresponding tip position delivered by our ground truth. In particular, we can see that the highest error is present at the beginning of the recorded time-window: it reaches a peak and then stabilizes. When starting the procedure, it is very likely that our drill bit hits the surface of the drill sleeve, thus causing additional shaking to the intrinsic drill vibrations. This happens also when the drill bit hits the surface of the bone. The shaking, as shown from the behavior of the position samples of our ground truth, is visible in particular along the x and y directions. These axes define a plane almost orthogonal to the direction of drilling, which is mostly affected by the vibration of the instrument, when hitting something. Once the surface is perforated, the movement of the drill bit is more constrained and this is reflected in a stabilization of both the estimated tip position and axis orientation and of the respective errors.

We could also noticed, that the highest errors occurs in case of inaccurate marker segmentation. When drilling, we could observe that because of the instrument vibrations, in particular when the instrument hits object surfaces, the image blurs. This affects in particular the detection of corner features, that is used both to validate the true presence of a marker and to recover the camera position. Mis-detection of one of more markers, together with inaccurate feature detection, do affect the result of the pose estimation.

4. CONCLUSIONS

We present a first implementation and evaluation of a novel camera-based solution for screw fixation guidance and motivate our choice for marker positioning on our custom-made drill sleeve. In order to evaluate the accuracy of our setup we exploited the Polaris tracking system, that allows tracking the position of the instrument in real time. In our experiments we achieved an accuracy of $1.60 \pm 1.22°$ and 2.03 ± 1.36 mm in the estimation of the axis orientation and the tip position respectively with our simple monocular setup. Analysis of the temporal behavior of the error curves let us conclude that the highest errors are encountered when just one marker is visible in the camera FOV or when just one marker is detected as a consequence of the increasing image blur. Outliers are encountered when the drill bit hits against the drill sleeve and the bone surface at the beginning of the drilling phase since the high vibrations impair correct marker recognition. The error stabilizes again after the perforation of the surface of the bone.

Our preliminary evaluation showed that further improvements are expected if 1) marker occlusion is explicitly addressed and 2) a marker detection algorithm is employed that can deal with image blur induced by the instrument vibrations. Moreover, we believe that marker tracking should be employed during the surface perforation phase. This is expected to reduce the number of outliers during this critical phase and still allow a valuable position feedback to the user for this transient phase.

REFERENCES

[1] D'lima, D. D., Urquhart, A. G., Buehler, K. O., Walker, R. H., and Colwell, C. W., "The effect of the Orientation of the Acetabular and Femoral Components on the Range of Motion of the Hip at Different Head-Neck Ratios," *The Journal of Bone and Joint Surgery (American)* **82**(3), 315–21 (2000).

[2] George, D. C., Krag, M. H., Johnson, C. C., Van Hal, M. E., Haugh, L. D., Grobler, L. J., et al., "Hole Preparation Techniques for Transpedicle Screws. Effect on Pull-Out Strength from Human Cadaveric Vertebrae," *Spine* **16**(2), 181 (1991).

[3] Diotte, B., Fallavollita, P., Wang, L., Weidert, S., Thaller, P., Euler, E., and Navab, N., "Radiation-Free Drill Guidance in Interlocking of Intramedullary Nails," *Medical Image Computing and Computer-Assisted Intervention–MICCAI* , 18–25 (2012).

[4] Magaraggia, J., Kleinszig, G., Graumann, R., Angelopoulou, E., and Hornegger, J., "A Video Guided Solution for Screw Insertion in Orthopedic Plate Fixation," in [*SPIE Medical Imaging 2013: Image-Guided Procedures, Robotic Interventions, and Modeling*], **8671** (2013).

[5] Yamazaki, T., Watanabe, T., Nakajima, Y., Sugamoto, K., Tomita, T., Yoshikawa, H., and Tamura, S., "Improvement of Depth Position in 2-d/3-d Registration of Knee Implants using Single-Plane Fluoroscopy," *Medical Imaging, IEEE Transactions on* **23**(5), 602–612 (2004).

[6] Acker, S., Li, R., Murray, H., John, P. S., Banks, S., Mu, S., Wyss, U., and Deluzio, K., "Accuracy of Single-Plane Fluoroscopy in Determining Relative Position and Orientation of Total Knee Replacement Components," *Journal of biomechanics* **44**(4), 784–787 (2011).

[7] Forman, C., Aksoy, M., Hornegger, J., and Bammer, R., "Self-Encoded Marker for Optical Prospective Head Motion Correction in MRI," *Medical Image Computing and Computer-Assisted Intervention–MICCAI* , 259–266 (2010).

[8] Lu, C., Hager, G., and Mjolsness, E., "Fast and Globally Convergent Pose Estimation from Video Images," *IEEE Transactions on Pattern Analysis and Machine Intelligence* **22**(6), 610–622 (2000).

[9] Otake, Y., Armand, M., Sadowsky, O., Armiger, R., Kutzer, M., Mears, S., Kazanzides, P., and Taylor, R., "An Image-Guided Femoroplasty System: Development and Initial Cadaver Studies," in [*SPIE Medical Imaging 2010: Visualization, Image-Guided Procedures, and Modeling*], **7625**.

[10] Magaraggia, J., Egli, A., Kleinszig, G., Graumann, R., Angelopoulou, E., and Hornegger, J., "Calibration of a camera-based guidance solution for orthopedic and trauma surgery," in [*Bildverarbeitung für die Medizin 2013*], 27–32, Springer (2013).

[11] Schmidt, J., Vogt, F., and Niemann, H., "Robust hand–eye calibration of an endoscopic surgery robot using dual quaternions," in [*Pattern Recognition*], 548–556, Springer (2003).